ELSEVIER

Polymer 44 (2003) 1437–1447

polymer

www.elsevier.com/locate/polymer

Reinforcement of model filled elastomers: characterization of the cross-linking density at the filler–elastomer interface by ^{1}H NMR measurements

J. Berriot[a], F. Martin[a], H. Montes[a,*], L. Monnerie[a], P. Sotta[b]

[a]*UMR 7615, ESPCI, 10 Rue Vauquelin, 75005, Paris, France*
[b]*Laboratoire de Physique des Solides Bat. 510, Université Paris Sud, 91405 Orsay, France*

Received 4 July 2002; received in revised form 4 November 2002; accepted 21 November 2002

Abstract

The cross-linking density at the filler–elastomer interface is analyzed by ^{1}H NMR measurements in model reinforced elastomers composed by grafted nanosilica particles and cross-linked ethylacrylate chains. We have focused our attention on the effect of introducing fillers on the relaxation of the bulk polymer matrix which is observed at long times ($t > 100$ μs). Measurements performed at high temperature ($T > T_g + 120$ K) have revealed that its relaxation is affected by the topological constraints existing at the particle surface. We deduce that the effect of particles in the bulk matrix can be interpreted as that of an homogeneous additional constraint density which increases proportionally to the surface area introduced in the matrix.

Keywords: Filled elastomers; Cross-link density; ^{1}H NMR measurements

1. Introduction

Elastomers are polymer networks composed by cross-linked polymer chains. Mechanical and swelling properties of these systems are controlled by the mesh size of the network, which depends on the density of topological constraints such as entanglements and cross-links [1–6].

When solid inclusions are added to such polymer systems, their mechanical and swelling properties are strongly changed. The so-called reinforced elastomers exhibit specific properties such as precocious non-linear elastic response or strong restrictions to swelling. The numerous studies devoted to filled elastomers have shown that their behavior is essentially controlled by two structural parameters (i) the particle/matrix interface and (ii) the dispersion state of the fillers. Two kinds of approaches have been developed to describe their behavior. The first one is derived from the physics of non-reinforced elastomers and consists in analyzing the influence of the interactions at the particle/matrix interface on the properties. The interactions at the interface are commonly described as additional topological constraints which change the mesh size of the polymer network and then the dynamical and elastic properties of polymer chains. According to their chemical nature (hydrogen bonds, covalent bonds, entanglements), their influence would vary with temperature or deformation rate. For instance, Görizt [7] has developed a model describing the temperature and deformation dependence of the modulus as a consequence of the variation of the topological constraint density at the interface with temperature and deformation.

The second kind of approach has been developed in order to understand the influence of geometrical parameters such as the arrangement or the shape of the fillers which are not taken into account in the previous models [8,9]. In this case, one analyzes the properties of the network composed by the fillers and its modifications with temperature or deformation rate. Kraus has developed [8] an approach which interprets the decrease of the modulus with increasing deformation ratio in terms of an 'aggregation–desaggregation' process occurring in the aggregates.

None of these approaches can describe the various properties measured on filled elastomers alone. A general frame unifying both kinds of concepts is still lacking. The main reason is that most of the studies were performed on industrial systems, in which a change of the interactions at the interface induces a change of the dispersion state, i.e. of

* Corresponding author. Tel.: +33-1-4079-4687; fax: +33-1-4079-7686.
E-mail address: helene.montes@espci.fr (H. Montes).

0032-3861/03/$ - see front matter © 2003 Elsevier Science Ltd. All rights reserved.
PII: S0032-3861(02)00882-0

the filler network. Thus, we have chosen to prepare model-reinforced systems which allow to vary these two parameters independently.

The samples were prepared according to the method developed by Ford et al. [22–25], which consists in polymerizing a colloidal suspension of grafted silica particles in acrylate monomers. We have shown [10] that it is possible to synthesize samples having the same particle/matrix interface properties and different dispersion states. In order to identify the relative importance of both structural parameters and to determine their possible influence on the mechanical behavior of the filled systems, it is necessary to characterize both the dispersion state and the interactions at the interface. The latter can be characterized by ^{1}H NMR spectroscopy. Many studies have shown [1–4,11–18] that this technique allows to measure the total topological constraint density (such as entanglements or cross-links) in polymeric systems. By comparing the transverse magnetization relaxation of reinforced and non-reinforced matrices, it is then possible to estimate the topological constraints density at the particle/matrix interface [16,17]. In this paper, we measure the topological constraint density at the particle/matrix interface in our model filled samples with ^{1}H NMR spectroscopy. We are able to determine the influence of the grafting density and of the nature of the coupling agent on the interaction strength at the interface.

This determination is based on the measure of the degree of averaging of nuclear interactions (namely here, dipolar couplings between ^{1}H nuclei) by molecular motions. This degree may then be easily related to the density of topological constraints at high temperature, typically 100 K above the glass transition temperature T_g. In this temperature range, polymer chains are in the fast motion regime, in which the non-zero average value of nuclear interactions provides the dominant contribution to nuclear relaxation and may be measured in a simple way with appropriate pulse sequences. For these reasons, we consider here the high temperature behavior.

The paper is organized as follows. We briefly recall the procedure used for the preparation of our filled elastomers. Then we present the theoretical background which relates the transverse magnetization relaxation to the topological constraint density at the particle/matrix interface. The results obtained on our filled elastomers are shown and discussed in Sections 3 and 4, respectively. We specifically analyze the influence of the dispersion state and of the chemical nature of the coupling agent molecules grafted onto the particle surface.

2. Experimental section

2.1. Sample preparation

2.1.1. The main steps of the filled elastomer synthesis

Spherical, weakly polydisperse particles of colloidal silica with varying diameter were prepared following the procedure developed by Stöber [20]. Some of them were prepared by Rhodia (Aubervilliers, France). Their mean size and polydispersity were characterized by Small Angle Neutron Scattering [10]. The structural features are given in Table 1.

Short silane molecules were grafted onto the silica particles surface using a dilute silica dispersion (2% (vol)). Three kinds of non-polar coupling agents were used: 3-trimethoxysilylpropylmethacrylate (TPM), 3-methacryloxy propyl dimethylchlorosilane (MCS) and acetoxyethyldimethylchlorosilane (ACS). For the TPM molecules, the grafting step is made in the initial Stober solution. The grafting reaction of the two coupling agent MCS and ACS requires to transfer the silica particles in an aprotic solvent (propylene carbonate). The amount of grafted coupling agent was determined by elemental analysis by comparing the carbon and silicon contents of the non-grafted and grafted silica particles.

The grafted silica particles are transferred to methanol and then to ethylacrylate monomers by successive dialysis following the procedure developed by Ford et al. [22–25] (for more details see Ref. [10]). Lastly, a photoinitiator (Irgacure (Ciba, France)) and a cross-linker—the diacrylate butanediol—are added to the dispersion in order to achieve the polymerization and the cross-linking respectively under UV illumination. Irrespective of the silica volume fraction, the concentration of initiator and cross-linker was kept equal to 0.1 wt% to monomer and 0.3% per mol of acrylate monomer, respectively. Filled elastomers were then prepared from colloidal solutions of colloidal grafted silica in acrylate monomers. The grafted silica dispersion in acrylate was syringed into a cell formed by two glass moulds. The cell was placed on a rotating plate and irradiated during 4 h by a fixed medium pressure 450 W Hg lamp. The polymerization and the cross-linking of the polyacrylate chains occur simultaneously.

2.1.2. Chemical structure of the particle/polymer interface

Chemical structure of the covering. TPM molecules have three reacting groups which can form a covalent bond either at the silica surface or with other TPM molecules. We have shown in Ref. [10] that polycondensation of the TPM molecules occurs around the silica surface. On the other hand, MCS and ACS grafters have only one group that can react with hydroxyl groups. In this case, there is no polycondensation between neighboring coupling agent molecules: MCS and ACS form brushes over the particle surface.

From the grafting density measured by elemental analysis, we can deduce the thickness e_{Graft} of the grafting layer applying the following relation

$$e_{\mathrm{Graft}} = r_0 \left(\sqrt[3]{1 + \frac{3\Gamma M_{\mathrm{mol}}^{\mathrm{G}}}{r_0 \rho^{\mathrm{G}} N_{\mathrm{a}}}} - 1 \right) \quad (1)$$

Table 1
Characteristics of the reinforced sample sets

Set name	Mean silica diameter (nm)	Graft type	Graft density (nm^{-2})	Dispersion state[a]	e_{Graft} (nm)
ACS/C	54	ACS	2	Very bad	–
MCS-I/C	45	MCS	1.6 ± 0.5	Good	0.52
MCS-II/H	50	MCS	2.8 ± 0.5	Bad	0.9
MCS-III/C	54	MCS	<1	Bad	<0.35
TPM-I/H	50	TPM	3.3 ± 1	Bad	1.07
TPM-II/H	54	TPM	7.8 ± 1	Bad	2.4
TPM-V/H	24	TPM	1.5 ± 0.5	Bad	1.3
TPM-III/C	80	TPM	10.5 ± 3	Good	1.3
TPM-VI/C	50	TPM	1.5 ± 0.5	Good	0.83

[a] From SANS measurements [10].

where M^{G}_{mol} and ρ^{G} are the molar weight and density of the grafter molecules, N_a the Avogadro number, r_0 the particle radius and Γ is the grafting density.

Interaction of the grafters with polyacrylate chains. Both TPM and MCS coupling agents have one methacrylate group which can react with acrylate monomers during the polymerization step. TPM or MCS silica particles are then covalently bonded to the acrylate matrix. On the contrary, the ACS coupling agent has no methacrylate ending. Thus, the ACS silica particles are not connected to the elastomer network.

Gel fraction measurements. The gel fraction G was measured for all the reinforced and non-reinforced samples. In this aim, the free chains contained in the samples were extracted using chloroform. The samples were washed with chloroform during 1 week, the solvent being replaced three times. The swollen samples were then carefully dried until their weight remains constant. The gel fractions of the polymer chains are deduced comparing the weight of the unwashed sample to the one after free chain extraction.

$$G = \frac{M_d - M_{Si}}{M_{ini} - M_{Si}}$$

where M_d and M_{ini} are the weight of the dried sample, respectively after and before extraction of the free chains, M_{Si} the weight of the silica particles dispersed in the sample.

We have observed gel fractions between 0.98 and 1 indicating that very few polymer chains are not connected to the polymer network.

Dispersion state quality. In a previous work we have shown that the final silica dispersion state depends on the procedure used to prepare the concentrated silica/acrylate dispersion from diluted dispersions, in order to obtain filled elastomer with varying silica volume fraction [10]. We have prepared several sets of filled elastomers differing by their particle size, the chemical nature of the grafter and the concentration procedure. Each set of samples corresponds to reinforced elastomers prepared from the same initial grafted silica solution with the same procedure of concentration. Each set of filled materials is composed of samples having volume fractions varying between 0.06 and 0.2. The dispersion state of the silica particles has been characterized by Small Angle Neutron Scattering [10]. This previous study has shown that we can consider three kinds of dispersion state labeled as 'good', 'bad' and 'very bad'. The label good means that the silica particles are arranged as spheres with repulsive interactions. Bad corresponds to quite disordered arrangement with many particle pairs. Very bad refers to samples containing fractal aggregates of particles. All the structural characteristics and the quality of the dispersion state for each sample set are given in Table 1.

2.2. NMR measurements

The NMR measurements were performed on the non-extracted samples containing less than 2% of free chains.

NMR measurements were performed on Brucker spectrometers operating at ^{1}H frequencies 100 MHz and 300 MHz, using a Bruker probehead with a 7 mm or 5 mm coil, respectively. The $\pi/2$ pulse duration was typically 4 μs. The transverse magnetization of the samples $M(t)$ was measured using the Hahn echo pulse sequence which refocuses the chemical shifts of various ^{1}H groups. The graphical representation of the Hahn echo pulse sequence is given below:

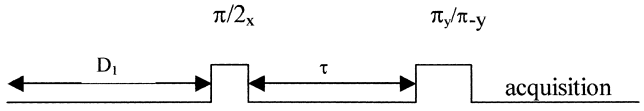

The measurements were done at 120 °C i.e. $T - T_g = 120$. The signal was observed over a time window 100 μs $< t <$ 10 000 μs typically. We obtained the relaxation curves by taking the amplitude of the echoes measured at the time 2τ, for varying τ values. For each value of τ, the amplitude of the echoes was averaged over 12 acquisitions.

Pseudo-solid spin-echoes (PSSE) were formed by applying the solid echo pulse train (or OW4 pulse sequence) which refocuses residual dipolar interactions.

The corresponding pulse sequence is described below:

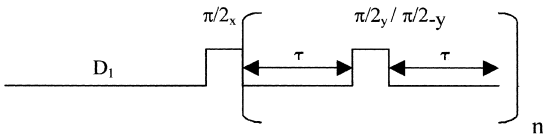

In this experiment, the signal is set exactly on resonance. The time interval between pulses was varied between 10 and 100 μs. n was taken equal to 62. The signal was averaged over 12 acquisitions.

For all measurements, a recycling delay D_1 of 4 s was chosen.

3. Theoretical section

We use ^{1}H NMR spectroscopy in order to compare the total cross-linking densities in our reinforced elastomers. The relaxation of the proton transverse magnetization is essentially determined by the averaging of ^{1}H–^{1}H dipolar magnetic interactions (which depends on molecular orientation) by molecular motions. In cross-linked elastomers, cross-links induce local constraints which restrict molecular reorientations in polymer chains. Polymer chain motions are thus anisotropic and dipolar spin interactions are not averaged to zero [1–4,19]. Thus, since the molecular dynamics varies with the topological constraints present in the sample, the relaxation of the transverse magnetization depends on cross-link and entanglement densities.

Several more or less complicated models have been developed in order to relate the transverse relaxation with the cross-linking and/or entanglement density [1,11–15]. The simplest model consists in representing the constraints associated with cross-links and/or entanglements as a fraction of points along the chains which are fixed in space. Then, the subchain formed by the N statistical segments located between two consecutive cross-links is considered to be isolated, i.e. free to reorient. In this picture, there are two well separated time scales: the intra-chain motions are fast while the average positions of the junction points are static, compared to the time scale defined by the NMR spin interactions. It is supposed that these intra-chain fast motions effectively average the couplings between remote groups. Assuming that each statistical segment carries an isolated pair of spins (two-spin approximation), the residual dipolar interaction within the chain can be expressed as [1,11,12]:

$$\overline{\omega_R} \propto \frac{\vec{R}^2}{N^2 a^2} \frac{3\cos^2\theta - 1}{2} \tag{2}$$

where $\vec{R}$ is the average distance between two consecutive cross-links, θ the angle between $\vec{R}$ and the magnetic field $\overrightarrow{B_0}$ and a is the length of a statistical segment. Since $R^2 = Na^2$, the residual interaction scales as the inverse of the statistical segment number within a subchain, which directly depends on the cross-link and/or the entanglement densities.

If all dipolar interactions are taken into account, the average of the residual dipolar interaction has to be extended to all pairs of spins. Cohen Addad [1] has shown that the N^{-1} scaling of $\overline{\omega_{\vec{R}}}$ is still valid in this case. Indeed, due to the r^{-3} dependence of the dipolar coupling on the distance r between spins, interactions between remote groups are much smaller than between close nuclei. Moreover, relative translational motions of topologically remote segments additionally average remote couplings even more efficiently than close ones, which reduces even more their average value and therefore, their contribution to the relaxation. As a result, the residual interaction is quite homogeneously distributed along the chain and the two-spin approximation can still be applied in a number of practical cases in order to get an estimate of N.

Within the above hypothesis, the time evolution of the transverse magnetization of the chain may be written:

$$M_{\vec{R}}(t) = \mathrm{Re}(M_0\, \mathrm{e}^{-t/T_2}\, \mathrm{e}^{\mathrm{i}\overline{\omega_{\vec{R}}}t}) \tag{3}$$

In an actual sample, the end-to-end vectors are distributed. The measured time relaxation of the transverse magnetization is the ensemble average of Eq. (3) over the chain end-to-end vector distribution.

The T_2 exponential factor comes from the fluctuating part of the dipole–dipole Hamiltonian. It corresponds to the irreversible (or incoherent) part of the time evolution.

The second oscillating contribution is due to the residual, non-zero interactions. It leads to a reversible (or coherent) time evolution which can be refocused by appropriate pulse sequences, such as the PSSE pulse sequence.

The separation of the time evolution in two factors lies on the hypothesis that chain motions (in between consecutive cross-links) are fast. This is valid at temperatures well above T_g. In this case, the time relaxation measured with a PSSE sequence corresponds essentially to the exponential term e^{-t/T_2} in Eq. (3). In particular, it is independent of the time interval τ between pulses in the sequence. Also, at T well above T_g, the dominant contribution to the relaxation is generally the coherent term, so that the incoherent contribution e^{-t/T_2} is often neglected [21].

Thus, at high enough temperatures, the relaxation of the transverse magnetization is essentially governed by the coherent processes, i.e. by the value of the residual interaction $\overline{\omega_{\vec{R}}}$, which depends directly on the cross-link and entanglement densities.

Let us consider the time relaxation of the transverse magnetization $M_1(t)$ and $M_2(t)$ in two different subchains containing N_1 and N_2 statistical units, respectively. From Eqs. (2) and (3), neglecting the irreversible T_2 contribution, we deduce that the relaxation $M_2(t)$ can be superimposed to $M_1(t)$ by applying the scaling factor $\lambda = N_1/N_2$ to the time scale.

It is then possible to estimate the relative degree of cross-linking in a polymer matrix by determining the shift factor to impose on the time scale in order to superimpose the relaxation curve to that measured on a reference elastomer matrix.

From Eq. (2), it is also possible to estimate an absolute number value of an 'effective' average subchain length, since the value of the static dipolar interaction within a given proton pair is known. When various samples with different cross-link densities are measured and the residual interaction (given by Eq. (2)) is extrapolated to zero cross-linking density, a finite N value is generally measured. This has been interpreted as the effect of trapped entanglements [14]. Thus, in order to take into account both kinds of topological constraints present in an elastomer matrix, namely cross-links and entanglements, the average sub-chain length may be taken as:

$$1/N = 1/N_c + 1/N_e \quad (4)$$

where N_c is given by the cross-link density ν_c and N_e is the number of statistical units between entanglements. Note that $1/N_e$ must be considered here to be an experimental parameter used to model the effect of entanglements. The relationship to the actual number of trapped entanglements and the microscopic description of their efficiency from the NMR point of view is not discussed here.

If the reference matrix is the entangled, non-cross-linked polymer matrix, then the shift factor to apply to superimpose the NMR curve measured on a cross-linked and uncross-linked sample writes: $\lambda = 1 + N_e/N_c$.

Note that Eq. (4) holds as the topological constraints, irrespective of their chemical and/or physical nature, are randomly distributed in the matrix. It is the case of unfilled cross-linked matrices, in which the entanglements and the cross-links are supposed to be homogeneously distributed in the polymer matrix. In this case, the quantity $1/N$ may be identified with the density of the corresponding constraints, so that Eq. (4) simply reads: $\nu_{total} = \nu_e + \nu_c$, with ν_c the cross-linking density and ν_e the entanglement density.

On the other hand, if some of the topological constraints are localized in few places in the elastomer matrix, a more precise analysis may be required. This could be the case in filled elastomers: the cross-links introduced by the particles in the elastomer matrix are localized at the particle surface and are then not randomly distributed. Let us examine two limiting cases. First, it may turn out that introducing filler particles results effectively in adding a uniform density ν_f of additional constraints (related to the presence of the filler particles). Then, a superposition principle would still hold in this case, provided that the total density of constraints $\nu_{total} = \nu_e + \nu_c + \nu_f$ is taken into account. On the other hand, the effect of the additional constraints may be strictly localized close to the filler particle surface, the bulk matrix remaining unaffected. In that case, no averaging of the constraint densities occurs, and the nuclear relaxation would be the superposition of two contributions: one corresponding to the bulk polymer matrix (characterized by a constraint density $\nu_e + \nu_c$), and another one corresponding to the region in the filler surface (characterized by a higher constraint density). Note that the polymer in the vicinity of the filler particles may even be solid. In that latter case, the superposition principle, applied to the whole relaxation function, would not hold anymore.

In summary, the nuclear relaxation in reinforced matrices has to be analyzed in two steps. First, the presence of a fastly relaxing component would indicate the presence of a fraction with a high degree of constraints within the polymer matrix, possibly related to the filler particle surface. Then, applying the superposition principle to the long time component in the relaxation (related to the bulk polymer matrix) would give a measure of the additional degree of topological constraints (with a density ν_G) within the bulk of the polymer matrix, related to the presence of the filler particles. The total topological constraint density (within the bulk polymer matrix) is then $\nu_{total} = \nu_e + \nu_c + \nu_G$.

We will apply these scaling properties of the NMR transverse relaxation signal to our series of reinforced elastomers in order to estimate the topological constraint density due to the particle/matrix covalent bonds.

4. Experimental results

4.1. Non-reinforced elastomer matrices

The relaxation of the transverse magnetization was measured at 120 °C, that is T_g(NMR) + 120 K.

At this temperature, the ^{1}H spectra (the Fourier transform of the transverse magnetization) consists in three poorly resolved lines (or groups of lines) of width 0.5–3.5 kHz, separated by about 1 ppm. One line corresponds to the CH groups, the second to the CH_2 and the third to the CH_3. A Hahn spin echo sequence has to be used in order to observe a relaxation function determined only by residual dipolar interactions, insensitive to the chemical shift differences between different groups.

In Fig. 1 the NMR signal measured through pseudo solid spin echoes is compared to the results obtained with a Hahn spin echo sequence. The former relaxes considerably slower than the latter. Also, the pseudo solid echo envelope does not depend on the time interval τ in the pulse sequence, in the range 10–100 μs. Both results indicate that the fluctuations contributing to the irreversible term e^{-t/T_2} are in the fast motion regime, and that no slow motion (at a time scale comparable to or slower than the time scale determined by the average dipolar interaction) contributes to the relaxation.

Thus, in this high temperature regime, we consider that the T_2 contribution to the transverse relaxation (i.e. the e^{-t/T_2} decay) is negligible compared to the coherent contribution.

It is observed that in this regime, the NMR relaxation curves (measured with the Hahn spin echo sequence)

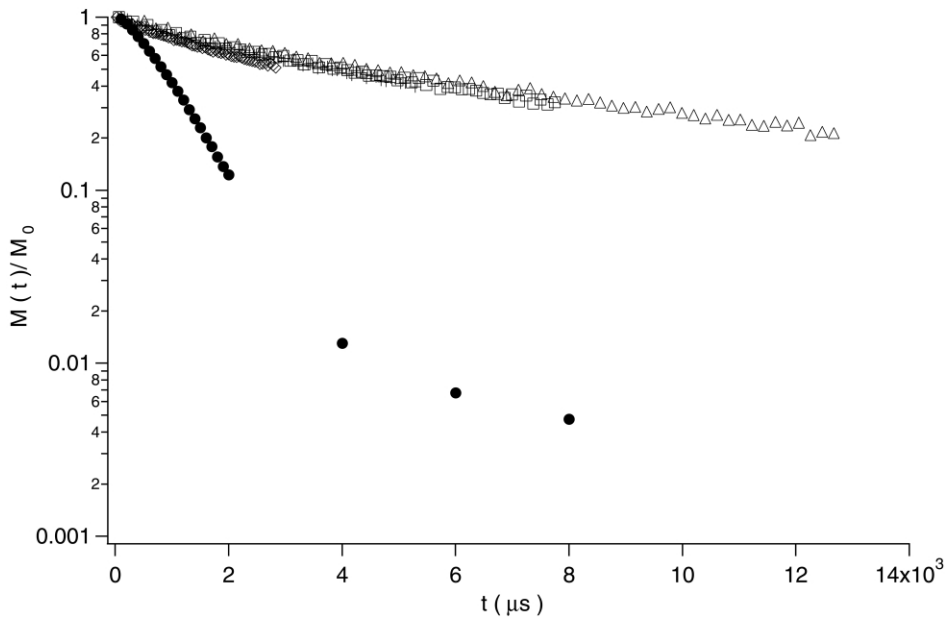

Fig. 1. Comparison of the relaxation of the transverse magnetization $M(t)/M_0$ measured at $T = 393$ K on a non-reinforced matrix EA-III by Hahn echoes (●) and pseudo-solid spin-echoes. The pseudo solid spin-echoes were measured for varying time τ of the OW4 pulse sequence: (◇): $\tau = 10$ μs, (+): $\tau = 20$ μs (□): $\tau = 30$ μs, (△): $\tau = 50$ μs.

obtained in pure elastomer matrices with various cross-linking densities obey the superposition properties mentioned above. The NMR measurements were performed on four reference pure ethylacrylate elastomer matrices (EA-0, EA-I, EA-II and EA-III) with different cross-linker concentrations. The corresponding cross-linker concentrations are given in Table 2. We have determined the shift factor λ_E to apply to the NMR signals of the three other elastomer matrices, so that they superimpose to the NMR curve measured on the uncross-linked EA-0 matrix taken as a reference. Assuming that all cross-linker molecules participate to the polymer network and that there are no free chain segments (dangling chains) in the network, the cross-link density ν_c is then proportional to $f\phi_{bd}/(1-\phi_{bd})$ where ϕ_{bd} is the molar fraction of cross-linkers and f their average functionality. We deduce the shift factor λ_E:

$$\lambda_E = 1 + \frac{\nu_c}{\nu_e} = 1 + \frac{f}{2}\frac{\phi_{bd}}{1-\phi_{bd}}N_e \qquad (5)$$

It is indeed observed that λ_E varies linearly with $\phi_{bd}/(1-\phi_{bd})$ (see Fig. 2).

The slope gives the statistical segment between two entanglements. Supposing a maximal functionality for the butanediol–diacrylate ($f = 4$), we find $N_e = 86$. This result is in almost quantitative agreement with the value obtained by dynamical mechanical measurements by Janacek et al. ($N_e = 80$) [26] or Tong et al. ($N_e = 110$) [27].

Table 2
Composition of the non-reinforced matrices

Sample	Cross-linker concentration (% per mol of acrylate)	Φ_{SI}^{w}
EA-0	0	0
EA-I	0.3	0
EA-II	0.6	0
EA-III	0.9	0

4.2. Reinforced samples

The same measurements were performed on the reinforced samples. At short times a fastly relaxing component is observed for systems containing MCS or TPM grafted silica particles. This feature shows the presence of a highly constrained polymer fraction within the matrix, corresponding to segments close to the particle surface. This fast relaxation contribution is larger at lower temperature and corresponds to polymer chains in the glassy state [28]. It amounts to less than 8% of the polymer matrix and is negligible at times longer than 100 μs. We have focused our attention to the long time component of the relaxation, observed in a time range between 100 μs and 2 ms, which is related to the bulk polymer matrix. This relaxation contribution is sensitive to the additional topological constraints introduced by the particles. We can estimate their density ν_G analyzing their influence on the shape of the relaxation at long time. In this aim the long time relaxation contribution was normalized by the amplitude of the Hahn echo measured at 100 μs and compared to the one measured on the non-reinforced matrices. Fig. 3 shows the NMR curves (measured with a Hahn spin echo sequence) obtained for the TPM-II/H family at $T_g + 120$ K. The NMR relaxation curves are located between the curves measured on the EA-I and EA-III reference matrices. We observed that the MCS-II/H and TPM-I/H samples are less cross-linked than the EA-II matrix. The cross-linking density of

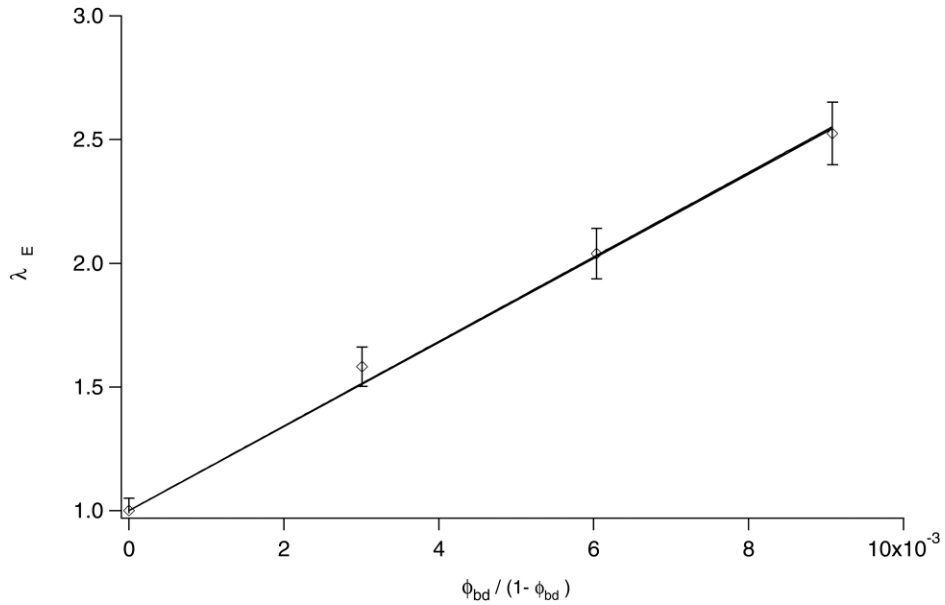

Fig. 2. Variation of the shift factor λ_E measured on the non-reinforced matrices versus $\phi_{bd}/(1-\phi_{bd})$ where ϕ_{bd} is the cross-linker concentration. The shift factor is determined here with respect to the uncross-linked matrix (the point at $\phi_{bd}=0$ in the curve).

the TPM-II/H is higher, but remains lower than that of the most cross-linked ethylacrylate matrix (EA-III) we have considered. As for the non-reinforced matrix with various cross-link densities, it is possible to superimpose the NMR curves measured in the reinforced samples onto the curve of a given non-reinforced matrix (taken as a reference), by applying a shift factor on the time scale.

The shift factors λ_{RE} were determined with respect to the EA-0 matrix, taken as a reference. The average topological constraint density ν_{tot} in the reinforced elastomer is given by:

$$\nu_{tot} = \nu_e + \nu_x \quad \text{with } \nu_x = \nu_c + \nu_G$$

ν_c and ν_G are the contributions due to the cross-linker agent (diacrylate butanediol) and the silica particles, respectively. The shift factor λ_{RE} is then given by: $\lambda_{RE} = (\nu_G + \nu_x)/\nu_e + 1$. The average mesh size of the reinforced samples may be deduced from the values λ_{RE} and compared to the average

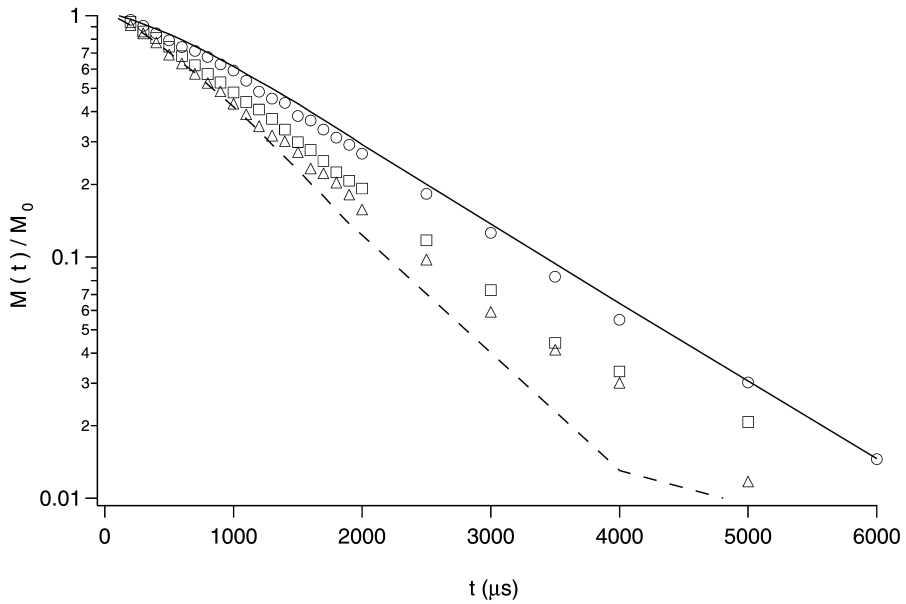

Fig. 3. Comparison of the time relaxation of the transverse magnetisation $M(t)/M_0$ measured by Hahn echoes at 393 K for different systems: in solid lines andin dashed lines the non-reinforced matrices EA-I and EA-III, respectively. The three other curves correspond to data measured on samples of the TPM-II/H set having different silica weigth fractions ϕ^w_{Si}: (○): $\phi^w_{Si}=0.11$, (□): $\phi^w_{Si}=0.21$, (△): $\phi^w_{Si}=0.29$.

distance between particles, which is given by

$$L = r_0\left(\left(\frac{\phi_{cp}}{\phi_{Si}^{vol}}\right)^{1/3} - 1\right)$$

where $\phi_{cp} = 0.64$ is the silica volume fraction at close packing and r_0 is the particle radius. For the TPM-II/H set, which corresponds to the most cross-linked samples compared to the other families, the mesh size is between 7 and 5 nm while the distance L varies between 52 and 21 nm. This example is representative of all reinforced samples, in which the mesh size is always smaller than the distance between particles.

The number of additional cross-links from the silica particles can then be evaluated from the quantity $\lambda_{RE} - \lambda_E$:

$$\lambda_{RE} - \lambda_E = \frac{\nu_G}{\nu_e} \quad (6)$$

The density of additional topological constraints due to the silica particles ν_G is given by the following expression:

$$\nu_G = N_{tc} N_{Si}/N_{EA}$$

N_{tc} is the number of topological constraints added by one silica particle. $N_{tc} = \langle f_{Si}\rangle S_0^{Si}$ with S_0^{Si} the surface of one silica particle and $\langle f_{Si}\rangle$ the average functionality of one silica particle (in nm^{-2}): $\langle f_{Si}\rangle$ is the product of the number of cross-link points $\langle f_{Si}^N\rangle$ at the silica surface with the functionality of each cross-link points f_{graft} ($\langle f_{Si}^N\rangle = \langle f_{Si}\rangle/f_{graft}$). N_{Si} is the number of silica particles per gram of filled elastomer: $N_{Si} = \phi_{Si}^w/\rho_{Si} V_0^{Si}$ where V_0^{Si} is the volume of one silica particle, ρ_{Si} is the silica density and ϕ_{Si}^w the silica particle weight fraction. N_{EA} is the number of ethylacrylate monomer: $N_{EA} = (1 - \phi_{Si}^w)N_a/M_0^{acrylate}$ with N_a the Avogadro's number and $M_0^{acrylate}$ the molar weight of the acrylate monomers. Finally, we find

$$\lambda_{RE} - \lambda_E = \frac{\langle f_{Si}\rangle}{2}\frac{\phi_{Si}^w}{1-\phi_{Si}^w}\frac{M_0^{acrylate} S_0^{Si}}{\rho_{Si} N_a V_0^{Si}} N_e \quad (7)$$

Fig. 4 shows the variation of $\lambda_{RE} - \lambda_E$ versus $\phi_{Si}^w/(1 - \phi_{Si}^w)$ for the four sets of reinforced elastomers, obtained from NMR measurements. For determining λ_E, we have assumed that all cross-linker molecules react with the acrylate monomers only and not with the grafters fixed on the particles. The value of λ_E is then deduced from the mole number of cross-linkers added per mole of ethylacrylate monomers (0.3%), and from the curve in Fig. 2, which gives the experimental variation of λ_E versus the cross-linker concentration in the non-reinforced matrices.

$\lambda_{RE} - \lambda_E = \nu_G/\nu_E$ varies typically between 0.1 and 1.1, which means that the density of constraints added by the particles is comparable to the density of both entanglements and cross-links.

We observe that, for each set of samples, $\lambda_{RE} - \lambda_E$ is proportional to $\phi_{Si}^w/(1 - \phi_{Si}^w)$, in agreement with Eq. (7). We have estimated $\langle f_{Si}^N\rangle$ from the value of the slope for each set of samples. We took $N_e = 86$ (according to the experimental results obtained in the non-reinforced matrices) and $f_{graft} = 2$. The values of $\langle f_{Si}^N\rangle$ obtained in this way are given in Table 3.

5. Discussion

As detected via NMR experiments at high T, the effect of introducing fillers is twofold: first, a solid-like signal appears at short times ($t < 100$ μs typically), which means that a fraction of the polymer matrix becomes solid. This fraction is most likely located close to the filler particle surface. This fraction however is quite small at high temperature. Secondly, the signal within the bulk matrix itself (100 μs $< t <$ 5 ms) is affected. It is shown here that it still obeys a superposition principle, which means that the effect on the NMR signal of particles in the bulk matrix may be interpreted in the same way as that of a homogeneous additional constraint density.

It is observed that the relaxation curves measured on non-reinforced matrices can be superimposed applying a shift factor on the time scale. Moreover, such superposition can be achieved between the relaxation curves measured on a reinforced elastomer and the one of a reference non-reinforced matrix. We deduced that the relaxation curves in a reinforced elastomer and in the equivalent non-reinforced matrix (containing the same total topological constraint density) superimpose at high temperature (typically $T = T_g + 120$ K). Fig. 5 shows the superimposition obtained with a sample of the TPM-V/H set containing the silica volume fraction of 0.16 and the non-reinforced matrix EA-II, both samples having the same $\nu_{tot}/\nu_e = 2.05$. This means that, at high temperature, the relaxation of the transverse magnetization is not sensitive to the heterogeneity of the spatial distribution of the topological constraints. In other words, the topological constraints localized at the interfaces have the same effect on the magnetization relaxation as the cross-links (and entanglements) homogeneously distributed in the matrix.

Moreover, the additional topological constraint density ν_G due to the introduction of particle is proportional to the

Table 3
The average functionality of the silica particles $\langle f_{Si}^N\rangle$ and the fraction α of grafters covalently bonded with acrylate monomers, deduced from Eq. (7) for each sample set

Set name	$\langle f_{Si}^N\rangle$ (nm^{-2})	α
ACS/C	0	–
MCS-I/C	2.25	1.4
MCS-II/H	1.05	0.375
MCS-III/C	0.15	–
TPM-I/H	1.1	0.33
TPM-II/H	2.8	0.36
TPM-V/H	1.05	0.7
TPM-III/C	1.7	0.17
TPM-VI/C	1.1	0.7

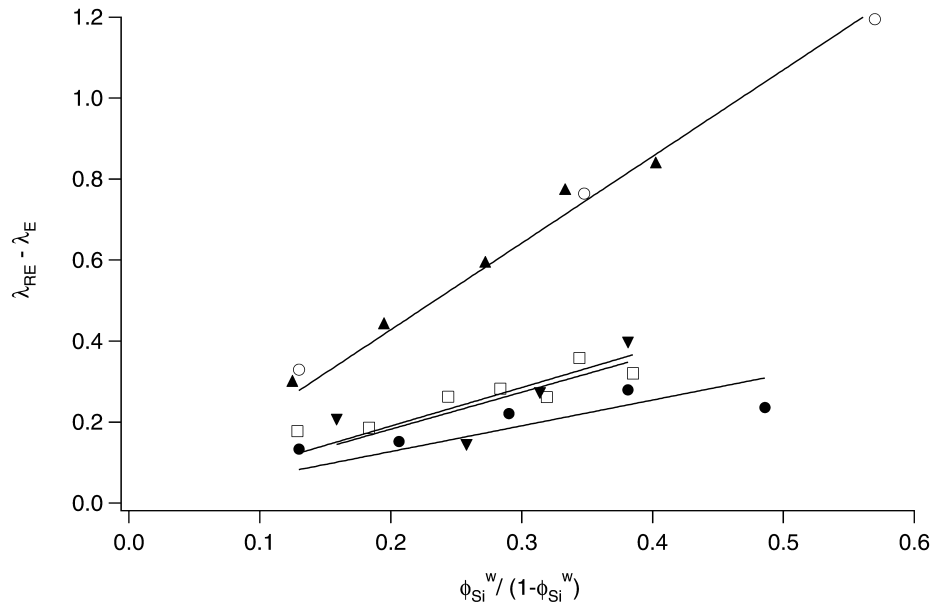

Fig. 4. Variation of $\lambda_{RE} - \lambda_E$ versus $\phi_{Si}^w/(1 - \phi_{Si}^w)$ for different reinforced elastomers: (○): MCS-I/C, (●): MCS-II/H, (□): TPM-I/H, (▲): TPM-II/H, (▼) TPM-III/H.

surface area via the factor $\phi_{Si}^w/(1 - \phi_{Si}^w)$. Thus, we may deduce that adding grafted particles does not change the reactivity of the cross-linker particles with the acrylate monomers. In a reinforced elastomer, far from the particle surface, the mesh size of the polymer network is controlled by the density of entanglements and cross-links $\nu_e + \nu_c$. This results was confirmed by swelling measurements [29]. We showed that beyond a distance of 5 nm from the particle surface, the swelling behavior of the polymer network is the same as the one observed in the non-reinforced matrix having the same density of entanglements and cross-links $\nu_e + \nu_c$. The mesh size of the polymer network depends on the cross-linker concentration only and is the same than that in the non-reinforced matrix with the same cross-linker concentration. In any case, the mesh size in the matrix is smaller than the average distance between particles. Then, beyond few nanometers (at maximum 5 nm), the elastomer matrix has the same elastic properties, whatever the silica concentration as shown by swelling measurements at equilibrium.

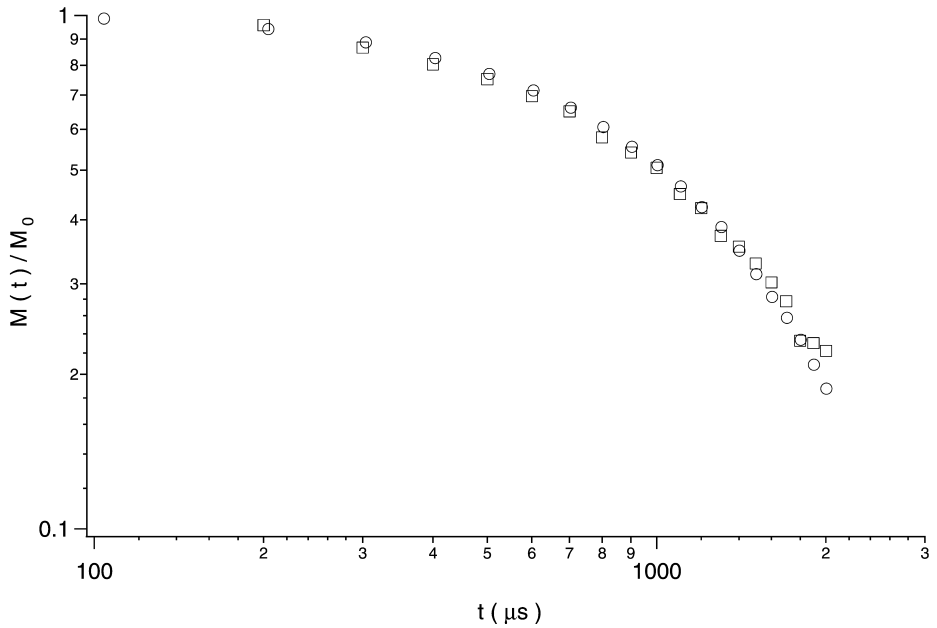

Fig. 5. Comparison of the time relaxation of the transverse magnetisation $M(t)/M_0$ measured by Hahn echoes at 393 K for a reinforced elastomer and a non-reinforced equivalent matrix that have the same topological constraints density as the reinforced sample. (□): TPM-V/H sample having a silica weight fraction $\phi_{Si}^w = 0.26$ such that $\nu_{tot}/\nu_e = 2.07$, (○): the non-reinforced matrix EA-II with $\nu_{tot}/\nu_e = 2.06$.

We observe that no additional topological constraint appears as ACS-silica particles are introduced in the elastomer matrix: the relaxation curves $M(t)/M_0$ measured on the ACS samples superimpose on the one measured on the reference matrix EA-I as shown in Fig. 6. On the other hand, the total topological constraint density ν_{tot} increases as the samples are reinforced with TPM or MCS silica, due to the additional cross-links at the particle/matrix interface. Irrespective of the dispersion state, the number of covalent bonds ν_G located at the particle/matrix interface is proportional to the total particle surface $\phi_{Si}^w/(1-\phi_{Si}^w)$, as it is also the case for MCS-III/C samples (not shown here), which contain aggregates.

The number of bonds at the particle/matrix interface depends on two structural parameters: the grafting density and the quality of the dispersion state. For the same dispersion states—see for example the TPM-I/H, TPM-II/H and MCS-II/H sets of samples—the average functionality of the particles increases with grafting density. However, the fraction α of grafters covalently bonded with acrylate monomers decreases as the grafting density increases. Assuming that the functionality of a grafter having reacted with acrylate monomers is maximum and equal to 2, α is given by $\langle f_{Si}^N \rangle / \Gamma$. The values of α in each sample set is given in Table 3. Comparing the results obtained from TPM-I/H, TPM-II/H and TPM-III/C, we observe that α drops down, or equivalently that most of the grafters cannot be reached and do not copolymerize with acrylate monomers as soon as the grafting density is higher than 3 nm^{-2}. This effect may come as well from the formation of loops at the particle surface: loops may not participate in the quantity ν_G (or have an efficiency lower than that of 'active' grafting points), and the fraction of loops may increase as the grafting density increases.

Furthermore, the density ν_G decreases as the quality of the dispersion state decreases. For instance, the $\langle f_{Si}^N \rangle$ varies inversely to the grafting density for the MCS-II/H samples (which contain small aggregates) and the MCS-I/C samples (which have a very good dispersion state). For bad dispersion states, part of the particle surface cannot be reached, leading to a decrease of the average interfacial topological constraint density $\langle f_{Si} \rangle$. As the dispersion state is good and the grafting density low—see the MCS-I/C and TPM-III/C samples—almost all the grafters are covalently bonded to acrylate monomers. In that case, the functionality of the grafters is maximum and equal to 2.

6. Conclusion

We have measured the additional topological constraints introduced by grafted silica particles in ethylacrylate elastomer matrices by ^{1}H NMR spectroscopy, in a high temperature regime (T_g + 120 K). The density of additional topological constraints increases proportionally to the surface area introduced in the matrix. This result shows that far from the particles, the polymer network is not affected by the covalent bonds connecting the polymer chains and the particles. Its mesh size is essentially controlled by the cross-linker concentration and the entanglement density. In further papers, we will analyze the influence of the topological constraints at the particle surface on the swelling and mechanical properties.

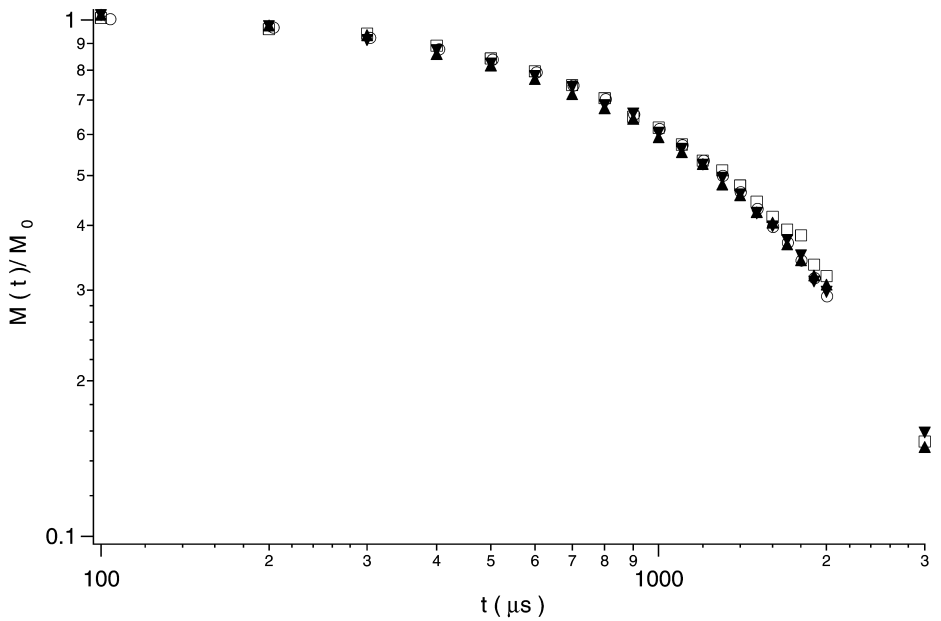

Fig. 6. Comparison of the time relaxation of the transverse magnetisation $M(t)/M_0$ measured by Hahn echos at 393 K on reinforced elastomers ofthe ACS/C set with the one mesaured on the reference m non-reinforced matrix EA-I. EA-I: (○); ACS/C: (□): $\phi_{Si}^w = 0.15$, (▲): $\phi_{Si}^w = 0.20$, (▼): $\phi_{Si}^w = 0.25$.

References

[1] Cohen Addad JP. NMR and fractal properties of polymeric liquids and gels. In: Emsley JW, Feeney J, Sutcliff LH, editors. Progress in NMR spectroscopy. New York: Pergamon Press; 1993. p. 25.
[2] Addad JPC, Pellicioli L, Nusselder JJH. Polym Gels Networks 1997; 5(2):201.
[3] Cohen Addad JP, Phan Thanh B, Montes H. Macromolecules 1997; 30:4374.
[4] Cohen Addad JP, Montes H. Macromolecules 1997;30:3678.
[5] Flory PJ. Principles of polymer chemistry. Ithaca, NY: Cornell University Press; 1969.
[6] Mark J, Erman B. Rubberlike elasticity—a molecular primer. New York: Wiley-Interscience; 1998.
[7] Maier PG, Görizt D. Kautschuk Gummi Kunstoffe 1996;49(1):18.
[8] Kraus G. J Appl Polym Sci-Appl Polym Symp 1984;39:75.
[9] Huber G, Vilgis TA, Heinrich G. J Phys Condens Matter 1996;8(29): L409.
[10] Berriot J, Montes H, Monnerie L, Martin F, Pychkout-Hinzten W, Meier G, Frielinghaus H. Submitted for publication.
[11] Brereton M. Macromolecules 1989;22:3667.
[12] Brereton M. Macromolecules 1991;24:206.
[13] Cohen Addad JP. J Chem Phys 1974;60:2440.
[14] Sotta P, Fülber C, Demco DE, Blümich B, Spiess HW. Macromolecules 1996;29:6222.
[15] Knoergen M, Menge H, Hempel G, Schneider H, Ries ME. Polymer 2002;43:4091.
[16] Litvinov VM, Steeman PAM. Macromolecules 1999;32:8476.
[17] Litvinov V, Vasiliev VG. Polym Sci USSR 1990;32:2231.
[18] Kulagina TP, Litvinov VM, Summanen KT. J Polym Sci Part B 1993; 31:241.
[19] Cohen Addad JP, Morel N. J de Phys III 1996;6(2):262.
[20] Stöber W, Fink A, Bohn E. J Colloid Interf Sci 1968;26:62.
[21] Sandakov GI, Smirnov LP, Sosikov AI, Summanen KT, Volkova NN, J Polym Sci, Part B 1994;32:1585.
[22] Sunkara HB, Jethmalani JM, Ford WT. Chem Mater 1994;6:362.
[23] Jethmalani JM, Ford WT. Chem Mater 1996;8:2138.
[24] Jethmalani JM, Ford WT. Langmuir 1997;13:3338.
[25] Jethmalani JM, Sunkara HB, Ford WT. Langmuir 1997;13:2633.
[26] Janacek J, Hrout J. J Polym Sci Polym Symp 1975;53:283.
[27] Tong JD, Leclère Ph, Doneux C, Bredas JL, Lazzaroni R, Jérôme R. Polymer 2001;42:3503.
[28] Berriot J, Montes H, Lequeux F, Monnerie L, Long D, Sotta P. J Non Cryst Solid 2002;307–310:719.
[29] Berriot J, Lequeux F, Montes H, Pernot H. Polymer 2002;43:6131.